

Revealing quantum spin liquid in the herbertsmithite $\text{ZnCu}_3(\text{OH})_6\text{Cl}_2$

V. R. Shaginyan,^{1,2,*} M. Ya. Amusia,^{3,4} J. W. Clark,^{5,6} G. S. Japaridze,²
A. Z. Msezane,² V. A. Stephanovich,⁷ Y. S. Leevik,⁸ and E. V. Kirichenko⁹

¹*Petersburg Nuclear Physics Institute of NRC "Kurchatov Institute", Gatchina, 188300, Russia*

²*Clark Atlanta University, Atlanta, GA 30314, USA*

³*Racah Institute of Physics, Hebrew University, Jerusalem 91904, Israel*

⁴*Ioffe Physical Technical Institute, RAS, St. Petersburg 194021, Russia*

⁵*McDonnell Center for the Space Sciences & Department of Physics,
Washington University, St. Louis, MO 63130, USA*

⁶*Centro de Ciências Matemáticas, Universidade de Madeira, 9000-390 Funchal, Madeira, Portugal*

⁷*Institute of Physics, Opole University, Oleska 48, 45-052, Opole, Poland*

⁸*National Research University Higher School of Economics, St. Petersburg, 194100, Russia*

⁹*Institute of Mathematics and Informatics, Opole University, Oleska 48, 45-052, Opole, Poland*

Based on experimental data and our theoretical analysis, we provide a strategy for unambiguous establishing of gapless quantum spin liquid state (QSL) in herbertsmithite and other materials. To clarify the nature of QSL, we recommend measurements of heat transport, low-energy inelastic neutron scattering and optical conductivity under the application of external magnetic field at low temperatures. We also suggest that artificially introduced inhomogeneity into $\text{ZnCu}_3(\text{OH})_6\text{Cl}_2$ can stabilize QSL, and serves as a test elucidating the contribution coming from impurities. We predict the results of these measurements in the case of gapless QSL.

PACS numbers: 64.70.Tg, 75.40.Gb, 78.20.-e, 71.10.Hf

In a geometrically frustrated magnet, spins are prevented from forming an ordered alignment, so that even at temperatures close to absolute zero they collapse into a liquid-like state called a quantum spin liquid (QSL). The herbertsmithite $\text{ZnCu}_3(\text{OH})_6\text{Cl}_2$ has been exposed as a $S = 1/2$ kagome antiferromagnet, and recent experimental investigations have revealed its unusual behavior [1–6]. The electrostatic forces balance for Cu^{2+} ions in a kagome structure makes them to occupy the distorted octahedral sites. In the herbertsmithite structure, magnetic planes formed by Cu^{2+} $S = 1/2$ ions are interspersed with nonmagnetic Zn^{2+} layers. In samples, Cu^{2+} defects occupy the nonmagnetic Zn^{2+} sites between the kagome layers with $x \simeq 15\%$ probability, thus introducing randomness and inhomogeneity into the lattice [7]. We suggest that the influence of this inhomogeneity on the properties of $\text{ZnCu}_3(\text{OH})_6\text{Cl}_2$ facilitates the frustration, and can be tested by varying x , as it is observed in measurements on the verdazyl-based complex $\text{Zn}(\text{hfac})_2(\text{A}_x\text{B}_{1-x})$ [8]. The experiments made on $\text{ZnCu}_3(\text{OH})_6\text{Cl}_2$ did not find any traces of magnetic order in it. Neither they have found the spin freezing down to temperatures of around 50 mK. This shows that the herbertsmithite is the best candidate to contain the above QSL. [1–6]. These results are confirmed by model calculations indicating that the ground state of kagome antiferromagnet is a gapless spin liquid [9–15]. On the other hand, it is shown that the intrinsic local spin susceptibility χ_{kag} vanished above $T \geq 10$ K and magnetic fields $B \geq 10$ T [16]. It has recently been suggested that there can exist a small spin-gap in the kagome layers [7, 16, 17], see also Refs [18, 19] for recent review. The results reported are based on both experimental facts and their

theoretical interpretation in the framework of impurity model [7, 17, 18]. The experimental data are derived from high-resolution low-energy inelastic neutron scattering on $\text{ZnCu}_3(\text{OH})_6\text{Cl}_2$ single-crystal. The impurity model assumes that the corresponding ensemble may be represented as a simple cubic lattice in the dilute limit below the percolation threshold. The model then suggests that in the absence of magnetic fields the bulk spin susceptibility χ exhibits a divergent Curie-like tail, indicating that some of the Cu spins act like weakly coupled impurities [7, 17, 18]. The same behavior is recently reported in a new kagome quantum spin liquid candidate $\text{Cu}_3\text{Zn}(\text{OH})_6\text{FBr}$ [20]. As a result, we observe a challenging contradiction between two sets of experimental data when some of them state the absent of a gap, while the other present evidences in the favor of gap.

Main goal of our letter is to attract attention to experimental studies of $\text{ZnCu}_3(\text{OH})_6\text{Cl}_2$ that can unambiguously reveal both the physics of QSL and the existence, or absence, of a possible gap in spinon excitations that form the thermodynamic, transport and relaxation properties. To unambiguously clarify the nature of QSL in herbertsmithite, we recommend the measurements of heat transport, low-energy inelastic neutron scattering and optical conductivity $\bar{\sigma}$ in $\text{ZnCu}_3(\text{OH})_6\text{Cl}_2$ subjected to external magnetic field. We suggest that the influence of impurities on the properties of $\text{ZnCu}_3(\text{OH})_6\text{Cl}_2$ can be tested by varying x . We predict results of these measurements.

To analyze the QSL properties theoretically, we employ the strongly correlated quantum spin liquid (SCQSL) model [9, 11, 13]. A simple kagome lattice may have a dispersionless topologically protected branch of the quasi-particle spectrum with zero excitation energy, that is the

so-called flat band [9, 11, 21, 22]. In that case a topological fermion condensation quantum phase transition (FCQPT) can be considered as QCP of the $\text{ZnCu}_3(\text{OH})_6\text{Cl}_2$, with SCQSL is composed of heavy fermions, or spinons, with zero charge and effective mass M^* , occupying the corresponding Fermi sphere with the Fermi momentum p_F . Consequently, the properties of insulating magnets coincide with those of heavy-fermion metals with one exception: Namely, typical insulator resists the electric current [9–13, 21].

At $B = 0$, contrary to the Landau Fermi liquid (LFL) behavior, where the effective mass M^* is approximately constant, this quantity becomes strongly temperature dependent, demonstrating the non-Fermi liquid (NFL) behavior [9]

$$M^*(T) \simeq a_T T^{-2/3}. \quad (1)$$

At finite T , the system transits to the LFL behavior, being subjected to the magnetic field

$$M^*(B) \simeq a_B B^{-2/3}. \quad (2)$$

The introduction of "internal" (or natural) scales greatly simplifies understanding the thermodynamic, transport and relaxation properties [9]. Namely, near FCQPT the effective mass $M^*(B, T)$ reaches its maximal value M_M^* at certain temperature $T_M \propto B$. Hence, to measure the effective mass and temperature, it is convenient to introduce the scales M_M^* and T_M respectively, see Fig. 1. This generates the normalized effective mass $M_N^* = M^*/M_M^*$ and the temperature $T_N = T/T_M$. Near FCQPT the normalized effective mass $M_N^*(T_N)$ can be well approximated by a simple universal interpolating function. The interpolation occurs between the LFL and NFL states, reflecting the universal scaling behavior of M_N^* [9]

$$M_N^*(y) \approx c_0 \frac{1 + c_1 y^2}{1 + c_2 y^{8/3}}. \quad (3)$$

Here, $y = T_N = T/T_M$, $c_0 = (1 + c_2)/(1 + c_1)$, where c_1 and c_2 are free parameters. The magnetic field B enters only in the combination $\mu_B B/T$, making $T_M \sim \mu_B B$. It follows from Eq. (3) that

$$T_M \simeq a_1 \mu_B B, \quad (4)$$

where a_1 is a dimensionless factor, μ_B is the Bohr magneton. Thus, in the presence of magnetic field the variable y becomes $y = T/T_M \sim T/\mu_B B$. Expression (4) permits to conclude that Eq. (3) describes the scaling behavior of the effective mass as a function of T and B : The curves M_N^* at different magnetic fields B merge into a single one in terms of the normalized variable $y = T/T_M$. Since the variables T and B enter symmetrically, Eq. (3) also describes the scaling behavior of $M_N^*(B, T)$ as a function of B at fixed T .

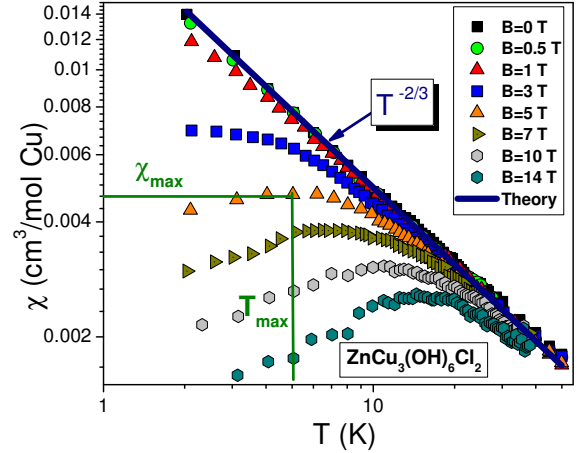


FIG. 1: (Color online) Measured temperature dependence of the magnetic susceptibility χ of $\text{ZnCu}_3(\text{OH})_6\text{Cl}_2$ from Ref. [1] at magnetic fields shown in the legend. Illustrative values of $\chi_{\max} \propto M_M^*$ and T_{\max} at $B = 3$ T are also shown. A theoretical calculation at $B = 0$ is plotted as the solid curve, which represents $\chi(T) \propto T^{-\alpha}$ with $\alpha = 2/3$ [10, 11, 13].

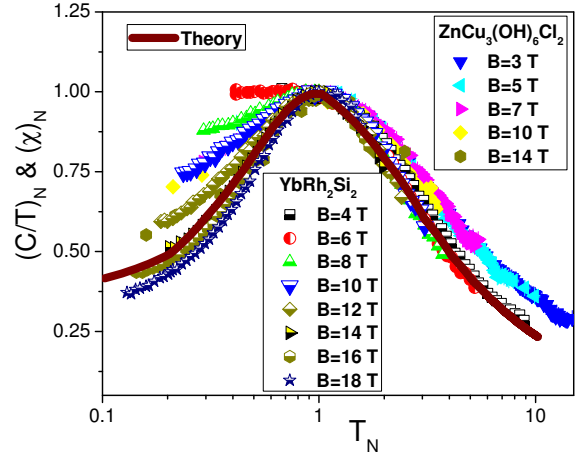


FIG. 2: Normalized susceptibility $\chi_N = \chi/\chi_{\max} = M_N^*$ versus normalized temperature $T_N = T/T_{\max}$ (see Eq. (3) and Fig. 1) extracted from the measurements of the magnetic susceptibility χ in magnetic fields B on $\text{ZnCu}_3(\text{OH})_6\text{Cl}_2$ [1] shown in Fig. 1. Normalized specific heat $(C/T)_N = M_N^*$ is extracted from the measurements of the specific heat C/T on YbRh_2Si_2 in magnetic fields B [23]. The corresponding values of B are listed in the legends. Our calculations made at $B \simeq B^*$ when the quasiparticle band is fully polarized are depicted by the solid curve tracing the scaling behavior of M_N^* [10, 13].

To examine the impurity model, we first refer to the experimental behavior of the magnetic susceptibility χ of herbertsmithite. It is seen from Fig. 1 that the magnetic susceptibility diverges $\chi(T) \propto T^{-2/3}$ in magnetic fields

$B \leq 1$ T [1, 11, 13], as shown by the solid line. In the case of weakly interacting impurities it is suggested that the low-temperature behavior of $\chi_{CW}(T) \propto 1/(T+\theta)$ can be approximated by a Curie-Weiss law [7, 16, 17], with θ being a vanishingly small Weiss temperature. However, given that $\chi(T) \propto T^{-2/3}$, the Curie-Weiss approximation is in conflict with both experiment [1] and theory [10, 11, 13]. Moreover, it is seen from Fig. 2 that normalized magnetic susceptibility χ behaves like the normalized heat capacity, extracted from measurements on YbRh_2Si_2 in high magnetic fields [23], and does not exhibit any gap. This observation confirms the absent of the spin gap in $\text{ZnCu}_3(\text{OH})_6\text{Cl}_2$ and invalidity of separating the contributions coming from the impurities. While χ_{kag} obeys $\chi_{\text{kag}}(T) = \chi(T) - \chi_{CW}(T)$, leading to $\chi_{\text{kag}}(T \rightarrow 0) \rightarrow 0$ and to the erroneous claim that a gap has been observed [16, 17]. To explain the observed behavior of χ , defining the real thermodynamic properties of $\text{ZnCu}_3(\text{OH})_6\text{Cl}_2$, it is necessary to consider the impurities and the kagome planes as an integral entity that forms QSL [9–14]. It is also suggested that mea-

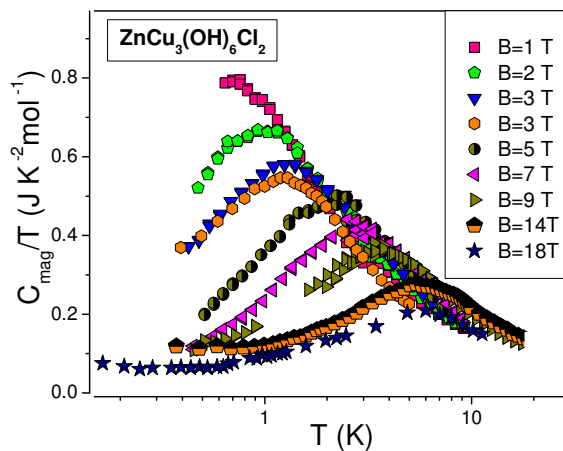


FIG. 3: (Color online) Specific heat C_{mag}/T measured on powder [2, 3] and single-crystal [4–6] samples of herbertsmithite is displayed as a function of temperature T for fields B shown in the legend.

surements of low energy inelastic neutron scattering on single crystals of herbertsmithite allow one to subtract the impurity scattering $S_{\text{imp}}(\omega)$ from the total scattering $S_{\text{tot}}(\omega)$ to obtain a measure of the intrinsic scattering $S_{\text{kag}}(\omega) = S_{\text{tot}}(\omega) - aS_{\text{imp}}(\omega)$, taking a as a fitting parameter. As a result, it is found that $S_{\text{kag}}(\omega) \rightarrow 0$ as ω decreases below the energy of 0.7 meV, leading to the gap existence. As we have shown above analyzing the magnetic susceptibility, such a subtraction leads to the erroneous conclusion that a gap has been found.

Let us consider somewhat further the inadequacy of the impurity model and its conclusion about spin gap existence when confronted with experimental findings. We

see from Fig. 1 that LFL behavior of the magnetic susceptibility χ is demonstrated at least for $B \geq 3$ T and low temperatures T . At such temperatures and magnetic fields the impurities should become fully polarized. Thus, assuming the impurities are fully polarized and hence do not contribute to χ , one has simply $\chi_{\text{kag}}(T) = \chi(T)$. Analogous behavior of the heat capacity follows from Fig. 3. LFL behavior of C_{mag}/T emerges under the application of the same fields. Consequently, we may conclude that at least at $B \geq 3$ T and $0.2 \leq T \leq 2$ K, the contributions to both χ and C_{mag}/T from the impurities are negligible; rather, one expects them to be dominated by the kagome lattice, exhibiting a spin gap in the kagome layers [7, 16, 17]. Thus, one would expect both $\chi(T)$ and $C_{\text{mag}}(T)/T$ to approach zero at $T \leq 2$ K and $B \geq 3$ T. It is clear from Figs. 1, 2, and 3, that this is not the case. These conclusions agree with recent experimental findings that the low-temperature plateau in local susceptibility identifies the spin-liquid ground state as gapless one [24], while recent theoretical analysis confirms the absence of a gap [15, 25]. Moreover, we suggest that the growing x , elevating randomness and inhomogeneity of the lattice and therefore facilitating the frustration of the lattice, can stabilize QSL. This observation can be tested in experiments on samples of herbertsmithite with different x under the application of magnetic field.

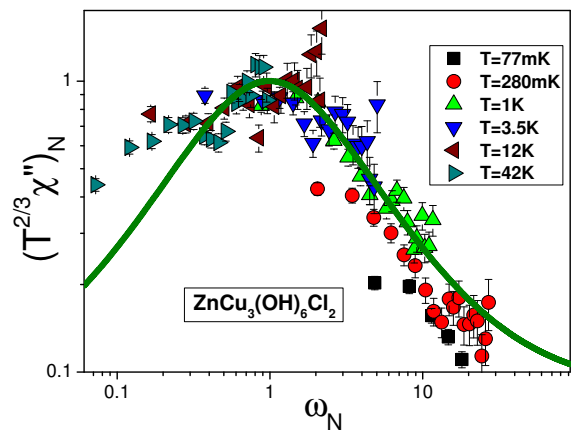


FIG. 4: (Color online) Scaling behavior of the normalized dynamic spin susceptibility $(T^{2/3}\chi'')_N$. Data are extracted from measurements on the herbertsmithite $\text{ZnCu}_3(\text{OH})_6\text{Cl}_2$ [1]. Solid curve: Theoretical calculations based on Eq. (6) [10, 12].

The same outcomes can be drawn from the results of neutron-scattering measurements of the dynamic spin susceptibility $\chi(\mathbf{q}, \omega, T) = \chi'(\mathbf{q}, \omega, T) + i\chi''(\mathbf{q}, \omega, T)$ as a function of momentum q , frequency ω , and temperature T . Indeed, these results play a crucial role in identifying the properties of the quasiparticle excitations involved.

At low temperatures, such measurements reveal that the corresponding quasiparticles – of a new type insulator – are represented by spinons, form a continuum, and populate an approximately flat band crossing the Fermi level [26]. The imaginary part $\chi''(T, \omega_1)$ satisfies the equation [10, 12]

$$T^{2/3}\chi''(T, \omega_1) \simeq \frac{a_1\omega_1}{1 + a_2\omega_1^2}, \quad (5)$$

where a_1 and a_2 are constants and $\omega_1 = \omega/(T)^{2/3}$. It is seen from Eq. (5) that $T^{2/3}\chi''(T, \omega_1)$ has a maximum $(T^{2/3}\chi''(T, \omega_1))_{\max}$ at some ω_{\max} and depends on the only variable ω_1 . Equation (5) confirms the scaling behavior of $\chi''T^{0.66}$ experimentally established in Ref. [1]. Similar to Eq. (3), we introduce the dimensionless function $(T^{2/3}\chi'')_N = T^{2/3}\chi''/(T^{2/3}\chi'')_{\max}$ and the (dimensionless) variable $\omega_N = \omega_1/\omega_{\max}$. In this case, Eq. (5) is modified to read

$$(T^{2/3}\chi'')_N \simeq \frac{b_1\omega_N}{1 + b_2\omega_N^2}, \quad (6)$$

with b_1 and b_2 are fitting parameters. Their role is to adjust the function on the right hand side of Eq. (6) to reach its maximum value 1 at $\omega_N = 1$. In such a situation it is expected that the dimensionless normalized susceptibility $(T^{2/3}\chi'')_N = T^{2/3}\chi''/(T^{2/3}\chi'')_{\max}$ exhibits scaling as a function of the dimensionless energy variable ω_N , as it is seen from Fig. 4. We predict that if measurements of χ'' are taken at fixed T as a function of B , then with respect to Eq. (2), we again obtain that the function $B^{2/3}\chi''(\omega)$ exhibits the scaling behavior with $\omega_N = \omega_1/\omega_{\max}$

$$(B^{2/3}\chi'')_N \simeq \frac{d_1\omega_N}{1 + d_2\omega_N^2}, \quad (7)$$

Similarly, d_1 and d_2 are fitting parameters adjusted such that the function $(B^{2/3}\chi'')_N$ reaches unity at $\omega_N = 1$. If the system is exactly at a FCQPT point, the above scaling is valid down to lowest temperatures. It would also be crucial to carry out the measurements of low energy inelastic neutron scattering on $\text{ZnCu}_3(\text{OH})_6\text{Cl}_2$ single crystals under the application of relatively high magnetic fields. Latter measurements permit to directly observe possible gap since in this case the contribution from supposed impurities is negligible, as we have seen above in the case of the spin susceptibility χ .

Measurements of heat transport are particularly salient in that they probe the low-lying elementary excitations of QSL in $\text{ZnCu}_3(\text{OH})_6\text{Cl}_2$ and potentially reveal itinerant spinons that are mainly responsible for the heat transport. Surely, the overall heat transport is contaminated by the phonon contribution; however, this contribution is hardly affected by the magnetic field B . SCQSL in herbertsmithite behaves like the electron liquid in HF metals – provided the charge of an electron is set to zero. As a

result, the thermal resistivity w of the SCQSL is given by [10, 13, 14]

$$w - w_0 = W_r T^2 \propto \rho - \rho_0 \propto (M^*)^2 T^2, \quad (8)$$

where $W_r T^2$ represents the contribution of spinon-spinon scattering to thermal transport, being analogous to the contribution AT^2 from electron-electron scattering to charge transport, and ρ is the longitudinal magnetoresistivity (LMR). Also, w_0 and ρ_0 are the residual thermal and electric resistivity respectively. Now, we consider

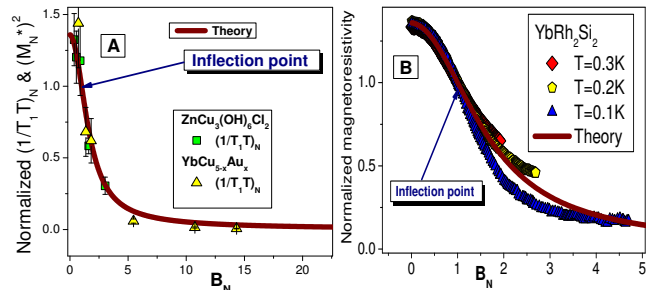


FIG. 5: (Color online) Panel (A). Normalized spin-lattice relaxation rate $(1/T_1T)_N$ at fixed temperature as a function of magnetic field. Data for $(1/T_1T)_N$ extracted from measurements on $\text{ZnCu}_3(\text{OH})_6\text{Cl}_2$ are shown by solid squares [27] and those extracted from measurements on $\text{YbCu}_{5-x}\text{Au}_x$ at $x = 0.4$, by the solid triangles [28]. The inflection point at which the normalization is taken is indicated by the arrow. Panel (B). Magnetic field dependence of the normalized magnetoresistance ρ_N , extracted from LMR of YbRh_2Si_2 at different temperatures [29] listed in the legend. The inflection point is shown by the arrow. In both panels (A) and (B), the calculated result is depicted by the same solid curve, tracing the scaling behavior of $W_r \propto (M^*)^2$ (see Eqs. (8) and (9)).

the effect of a magnetic field B on the spin-lattice relaxation rate $1/(T_1T)$. Fig. 5 A shows the normalized spin-lattice relaxation rate $1/(T_1T)_N$ at fixed temperature versus magnetic field B . It is seen that increasing of B reduces progressively $1/(T_1T)$. Also, the curve in Fig. 5 A has an inflection point at some $B = B_{\text{inf}}$, marked by the arrow. To detect the scaling behavior in this case, we normalize $1/(T_1T)$ by its value at the inflection point, while the magnetic field is normalized by B_{inf} . Taking into account the relation $1/(T_1T)_N \propto (M^*)^2$, we expect that a strongly correlated Fermi system located near its QCP would exhibit the similar behavior of $1/(T_1T)_N$ [9, 10, 13, 14]. Significantly, Fig. 5 A shows that the herbertsmithite $\text{ZnCu}_3(\text{OH})_6\text{Cl}_2$ [27] and the HF metal $\text{YbCu}_{5-x}\text{Au}_x$ [28] do exhibit the same behavior for the normalized spin-lattice relaxation rate. As seen from Fig. 5 A for $B \leq B_{\text{inf}}$ (or $B_N \leq 1$) the normalized relaxation rate $1/(T_1T)_N$ depends weakly on the magnetic

field, while it diminishes at the higher fields [9, 10, 13, 14] according to

$$W_r \propto 1/(T_1 T)_N \propto (M^*)^2 \propto B^{-4/3}. \quad (9)$$

Thus, we predict that the application of a magnetic field B leads to a crossover from NFL to LFL behavior and to a significant reduction in both the relaxation rate and the thermal resistivity, as the normalized LMR of YbRh_2Si_2 does, see Fig. 5 B.

Our next step is analysis of the herbertsmithite low-frequency optical conductivity $\bar{\sigma}$. To avoid the contribution of phonon absorption into the conductivity, we consider low temperatures T and frequencies ω [30]. This is because the above contribution becomes substantial at elevated T and ω [31]. In the case of QSL the optical conductivity is given by [30]

$$\bar{\sigma}(\omega) \propto \omega \chi''(\omega) \propto \omega^2 (M^*)^2. \quad (10)$$

It follows from Eq. (10) that $\bar{\sigma}(\omega) \propto \omega^2$, and that behavior is consistent with experimental facts obtained in measurements on $\text{ZnCu}_3(\text{OH})_6\text{Cl}_2$ and $\text{EtMe}_3\text{Sb}[\text{Pd}(\text{dmit})_2]_2$ representing the best candidates for identification as a material that hosts QSL [31, 32]. It is seen from Eqs. (1) and (10), that at elevated temperatures the low-frequency optical conductivity is a decreasing function of T . This observation is consistent with the experimental data [31], see also [33]. It also follows from Eqs. (2) and (10) that $\bar{\sigma}(\omega)$ diminishes under the application of magnetic fields. This observation seems to contradict the experimental results since no systematic magnetic field dependence is observed [31]. To elucidate the magnetic field dependence of $\bar{\sigma}(B)$, we note that measurements of $\bar{\sigma}(B)$ have been taken at 6 K and the magnetic fields $B \leq 7$ T [31]. In such a case the system is still in the transition regime and does not enter into the LFL state at which the effective mass M^* is given by Eq. (2) [9]. Therefore, in this case the effective mass behavior is determined by Eq. (1), rather than by Eq. (2), and the $\bar{\sigma}(B)$ dependence cannot be observed. As a result, we predict that the B -dependence of $\bar{\sigma}$ can be observed at $B \simeq 7$ T provided that $T \leq 1$ K. In that case, as it seen from Fig. 3, at $T \leq 1$ K the effective mass $M^* \propto C_{\text{mag}}/T$ is a diminishing function of the applied magnetic field. Thus, we predict that $\bar{\sigma}(B)$ diminishes at growing magnetic fields, as it follows from Eqs. (2) and (10). We note that the above experiments on measurements of the heat transport and optical conductivity can be carried out on samples with different x . As a result, these experiments allow us to test the influence of impurities on the value of the gap. We predict that at moderate $x \sim 20\%$ QSL remains robust, for both the inhomogeneity and randomness facilitate frustration.

In summary, the main message of our paper is to suggest performing the above discussed heat transport, low energy inelastic neutron scattering, and optical conductivity $\bar{\sigma}$ measurements on $\text{ZnCu}_3(\text{OH})_6\text{Cl}_2$ subjected to

external magnetic fields. We have suggested that growing x , characterizing % of the Zn sites that are occupied by Cu, can facilitate the frustration of the lattice, and thus can stabilize QSL. This observation can be tested in experiments on samples of herbertsmithite with different x . Considered measurements can give an unambiguous answer if a real gap in spinon excitations, determining the thermodynamic, transport and relaxation properties of insulating magnets, exists, or does not exist, and how it depends on impurities. Such measurements pave a new avenue for technological applications of the magnets.

We are grateful to V.A. Khodel for valuable discussions. This work was partly supported by U.S. DOE, Division of Chemical Sciences, Office of Basic Energy Sciences, Office of Energy Research. JWC acknowledges support from the McDonnell Center for the Space Sciences, and expresses gratitude to the University of Madeira and its branch of Centro de Investigação em Matemática e Aplicações (CIMA) for gracious hospitality during periods of extended residence.

* Electronic address: vrshag@thd.pmpi.spb.ru

- [1] J.S. Helton *et al.*, Phys. Rev. Lett. **104**, 147201 (2010).
- [2] J.S. Helton *et al.*, Phys. Rev. Lett. **98**, 107204 (2007).
- [3] M.A. deVries *et al.*, Phys. Rev. Lett. **100**, 157205 (2008).
- [4] T.H. Han *et al.*, Phys. Rev. B **83**, 100402(R) (2011).
- [5] T.H. Han, S. Chu, and Y.S. Lee, Phys. Rev. Lett. **108**, 157202 (2012).
- [6] T.H. Han *et al.*, arXiv:1402.2693 (2014).
- [7] T.H. Han *et al.*, Phys. Rev. B **94**, 060409(R) (2016).
- [8] H. Yamaguchi *et al.*, Scient. Rep. **7**, article number: 16144 (2017) doi:10.1038/s41598-017-16431-0.
- [9] V.R. Shaginyan, M.Ya. Amusia, A.Z. Msezane, and K.G. Popov, Phys. Rep. **492**, 31 (2010).
- [10] M.Ya. Amusia, K.G. Popov, V.R. Shaginyan, and V.A. Stephanovich, *Theory of Heavy-Fermion Compounds*, Springer Series in Solid-State Sciences **182** (2015).
- [11] V.R. Shaginyan, A.Z. Msezane, and K.G. Popov, Phys. Rev. B **84**, 060401(R) (2011).
- [12] V.R. Shaginyan, A.Z. Msezane, K.G. Popov, and V.A. Khodel, Phys. Lett. A **376**, 2622 (2012).
- [13] V.R. Shaginyan *et al.*, Europhys. Lett. **97**, 56001 (2012).
- [14] V.R. Shaginyan *et al.*, Europhys. Lett. **103**, 67006 (2013).
- [15] H.J. Liao *et al.*, Phys. Rev. Lett. **118**, 137202 (2017).
- [16] M. Fu, T. Imai, T.H. Han, and Y.S. Lee, Science **350**, 655 (2015).
- [17] T. Imai, M. Fu, T.H. Han, and Y.S. Lee, Phys. Rev. B **84**, 020411(R) (2011).
- [18] M.R. Norman, Rev. Mod. Phys. **88**, 041002 (2016).
- [19] Y. Zhou, K. Kanoda, and T.-K. Ng, Rev. Mod. Phys. **89**, 025003 (2017).
- [20] Z. Feng *et al.*, Chin. Phys. Lett. **34**, 077502 (2017).
- [21] V.R. Shaginyan *et al.*, J. Low Temp. Phys. **189**, 410 (2017).
- [22] D. Green, L. Santos, and C. Chamon, Phys. Rev. B **82**, 075104 (2010).
- [23] P. Gegenwart *et al.*, New J. Phys. **8**, 171 (2006).
- [24] M. Gomišek *et al.*, Phys. Rev. B **94**, 024438 (2016).

- [25] H.J. Liao *et al.*, Phys. Rev. Lett. **118**, 137202 (2017).
- [26] T.H. Han *et al.*, Nature **492**, 406 (2012).
- [27] T. Imai *et al.*, Phys. Rev. Lett. **100**, 077203 (2008).
- [28] P. Carretta, R. Pasero, M. Giovannini, and C. Baines, Phys. Rev. B **79**, 020401(R) (2009).
- [29] P. Gegenwart *et al.*, Science **315**, 969 (2007).
- [30] V.R. Shaginyan *et al.*, J. Low Temp. Phys. **191**, 4 (2018).
- [31] D.V. Pilon *et al.*, Phys. Rev. Lett. **111**, 127401 (2013).
- [32] A. Pustogow *et al.*, arXiv:1803.01553.
- [33] T.-K. Ng and P. A. Lee, Phys. Rev. Lett. **99**, 156402 (2007).